


Design and implementation of smart integrated hybrid Solar-Darrieus wind turbine system for in-house power generation

Firas Basim Ismail Alnaimi^{1,2,*} , Hussein A. Kazem^{1,2}, Ariff Bin Alzakri¹, and Abdulaziz Mohammed Alatir¹

¹ Smart Power Generation Unit, Institute of Power Engineering (IPE), University Tenaga Nasional (UNITEN), Kajang, 43000, Malaysia

² Faculty of Engineering, Sohar University, PO Box 44, Sohar PCI 311, Oman

Received: 28 August 2023 / Revised: 6 September 2023 / Accepted: 7 September 2023

Abstract. This paper presents the design and development of an integrated hybrid Solar-Darrieus wind turbine system for renewable power generation. The Darrieus wind turbine's performance is meticulously assessed using the SG6043 airfoil, determined through Q-blade simulation, and validated via comprehensive CFD simulations. The study identifies SG6043 as the optimal airfoil, surpassing alternatives. CFD simulations yield specific coefficients of power (0.2366) and moment (0.0288). The paper also introduces a hybrid prototype, showcasing of 10 W photovoltaic module and improved turbine performance with the SG6043 airfoil. The focus extends to an optimized hybrid PV solar-wind system seamlessly integrated with IoT technology for remote monitoring. Addressing weather challenges, the research suggests blade shape optimizations via Q-blade and an IoT-based solution leveraging the ESP32 Wi-Fi module. Theoretical results project electrical energy generation ranging from 0.88 kW on March 14, 2023, to 0.06 kW on February 20, 2023. Darrieus wind turbines, experiencing increased blade drag, require less lift to operate. Experimental and theoretical results converge well, affirming the model's reasonable assumptions. Beyond advancing renewable energy technologies, this research sets the stage for future investigations aimed at enhancing the efficiency and capabilities of hybrid wind-solar PV systems.

Keywords: Integrated hybrid system / Solar-Darrieus wind turbine / renewable energy / IoT-based monitoring / efficiency enhancement

1 Introduction

The increasing global focus on energy demand has driven movements towards carbon neutrality and the adoption of renewable energy sources. Conventional energy sources, though historically relied upon for their high energy density, raise environmental concerns due to carbon and greenhouse gas emissions. As projected energy demand is set to rise by 56% from 2010 to 2040, the significance of renewable energy power plants has grown [1]. Malaysia has witnessed notable growth in photovoltaic (PV) systems, leveraging its hot and humid climate to harness substantial solar radiation [2]. Wind energy utilization in Malaysia has gained attention in recent years as the country seeks to diversify its energy mix and reduce its dependence on fossil fuels. While Malaysia has traditionally focused on hydroelectric and fossil fuel-based energy sources, wind

energy is gradually being explored and integrated into its power generation landscape [3]. The Darrieus wind turbine is a type of “vertical-axis wind turbine” (VAWT) known for its distinctive helical or “eggbeater” shape. Unlike traditional “horizontal-axis wind turbines” (HAWTs), which have their blades oriented parallel to the ground, Darrieus turbines have blades that rotate around a vertical axis, perpendicular to the ground. This unique design of the blades offers several advantages and challenges in harnessing wind energy such as [4,5]: (i) the vertical plane, allowing them to capture wind from any direction without needing to constantly rotate to face the wind, (ii) an aerodynamic airfoil shape and are arranged in a helical pattern around the central vertical axis. This design enables self-starting capabilities and helps in capturing wind energy from various wind speeds and directions, (iii) the blades are tall compared to their width, allowing them to capture higher altitude wind currents effectively, (iv) used in smaller-scale applications, such as residential or community-based installations. The motivation behind

* e-mail: Firas@uniten.edu.my

designing a solar-darius hybrid wind turbine system for indoor power generation stems from the urgent need to address the challenges posed by conventional energy sources and their associated environmental impacts. Working with a hybrid solar-wind system may be a promising solution because it harnesses the complementary nature of solar and wind energy to ensure stable and sustainable energy generation. These hybrid systems will be suitable for residential and small-scale applications. It must be taken into consideration that the wind energy industry faces many challenges, including: low wind speeds and variability, which makes continuous and stable electricity generation using wind energy something that cannot be achieved in natural conditions. However, studies point to potential solutions to increase the viability of wind energy through turbine design analysis. To address these concerns and improve renewable energy systems, a hybrid approach that combines wind and solar power has emerged [6]. Solar energy has several characteristics that make it suitable for generating energy. It is a renewable resource, meaning it is constantly renewed by the sun. As long as the sun exists, we can harness its energy to generate energy. It is also an abundant energy source as it radiates a huge amount of energy every day, much more than humanity currently consumes. This makes solar energy an almost limitless resource [7]. Also, solar energy is clean and environmentally friendly: generating solar energy does not produce any greenhouse gas emissions or air pollutants. It is a clean and environmentally friendly energy source. Solar energy systems provide energy independence to homeowners, businesses, and even entire regions. They reduce dependence on fossil fuels and centralized energy grids [8]. Considering the crucial role of energy in economic development, welfare, and overall quality of life, exploring renewable energy alternatives becomes imperative [9]. Wind and solar energy sources offer clean options, and a hybrid system combining both ensures continuous power output. However, weather variations pose challenges to both standalone renewable sources and hybrid systems, affecting their stability and voltage production [10]. The current study aims to improve voltage production and overall system stability by optimizing the blade shape. Using the Darius wind turbine as a case study, this paper will analyze the operating mechanism, factors that affect its performance, and its self-starting abilities to improve the solar-wind hybrid power generation system in Malaysia. Models of the relevant equations are derived using Computational Fluid Dynamics (CFD) and Q-blade to simulate turbines. A hybrid solar-wind power generator with enhanced power production capabilities and self-starting ability is the ultimate goal. There is also a discussion of the experimental design and validation. Based on the researcher's knowledge, no previous studies have addressed this new design trend.

2 Literature review

The working principal of a Darrieus VAWT was noted as a wind turbine that uses the lift force generated to create the movement and power generation in contrast to the

Savonius VAWT which uses the drag force generated from the wind. Darrieus wind turbines commonly have two or three blades and are alternatively known as “eggbeaters” due to its C-shaped rotor blades creating the shape of an eggbeater. However, this design was the turbine that was patented in 1931, where the evolution and innovation of the technology has brought upon various designs such as the H-Darrieus and the helical Darrieus. The turbine has good efficiency but low reliability from the large torque ripple and cyclic stress produced on the tower [11].

A commonly known fact from the research found is that the Darrieus turbine requires an exterior power source to assist in the initiation of rotation of the turbine because of its low starting torque. Therefore, among the studies conducted, the research on the self-starting ability of the turbine has been conducted to tackle this limitation of this turbine. A parameter that is frequently discussed on the self-starting of the system is the “tip speed ratio” (TSR) which is described as the relation between the wind speed and the speed of the tips of the turbine. This parameter plays a major role in the efficiency of the turbine. Another important parameter considered in the design of the blades is the angle of attack, α , which represents the angle between the body's reference line and the oncoming flow. This angle affects the lift and drag experienced on the turbine which indefinitely affects the performance of the wind turbine. However, it was also found that the low TSRs are not suitable for the operation of the turbine as flow separation destabilizes the rotation of the blade. It was also determined that there is still potential for the advancement of the wind turbine through rotor arrangements and wind farms computational analysis [12,13].

Aside from self-starting ability, efficiency and optimization of the wind turbine were discussed in the studies, with CFD analysis used in the majority of cases. An unsteady (transient) “Reynolds-Averaged-Navier-Stokes” (URANS) method was used as well as a quadratic equation based on a regression model and a rotational degree of freedom solver (6DOF). Obtaining an accurate prediction of the turbine's behavior during startup requires the correct distribution of the lift and drag forces [14,15].

In Malaysia, the design of the hybrid energy system is more distinct and clear when dealing with wind energy due to the low average annual speed that the country experiences. A hybrid solar-wind power generator used to power street lighting has been designed and developed [16]. In such designs, the engineering of solar panels is taken into account, as well as the optimization of wind turbines and their systems, with the aim of producing the maximum amount of energy possible. The question that always arises in such studies is the effect of deflected flow because it reduces the power output capacity of the power generator [17].

A hybrid power generation system has the potential to address the challenge of low mean annual wind speeds in Malaysia. Notably, research has been undertaken to optimize such a hybrid power generation system. In a related context, a study in Zimbabwe conducted optimization efforts for a hybrid power generation system that powered a streetlight using both solar and wind sources [18]. This hybrid renewable energy system design encom-

Table 1. Benchmark studies in literature.

References	F1	F2	F3	F4	F5
[20]	✓	✓			✓
[21]	✓	✓			✓
[19]	✓	✓		✓	
[22]					
[23]	✓	✓			
[24]	✓		✓		
[25]	✓				
[26]		✓		✓	✓
[18]					
[27]	✓				
[28]	✓		✓	✓	✓
[29]	✓		✓		✓
[30]	✓		✓	✓	✓
[31]	✓	✓			✓

passed essential components, including a wind turbine, photovoltaic modules, a charge controller, a battery bank, and lighting units, all aimed at efficiently powering a 160W streetlight. The outcomes of the experiment demonstrated a notable reduction of 38.75% in energy storage requirements. Additionally, there was an overall cost reduction of 14.4% when compared to conventional standalone streetlights. Furthermore, the hybrid system design achieved an impressive reliability rate of 98.4%. The associated cost was approximately USD 435, accompanied by a leveled energy cost of 17.5 cents/kWh. These results highlight the potential advantages and effectiveness of the hybrid system design in addressing energy storage needs, reducing costs, and enhancing overall reliability when compared to traditional single-source systems.

Additional research, such as the investigation into a Savonius-Darrieus hybrid system, can also contribute valuable insights to the advancement of hybrid systems. An illustrative case in point is a study conducted by [19]. This study delved into the impact of the number of blades on a VAWT through computational analysis. The findings of this study revealed that a configuration comprising a two-bladed Savonius rotor and a three-bladed Darrieus rotor exhibited enhanced self-starting capabilities. Specifically, the values of 0.41 for the “maximum coefficient of power” (C_p) and 2.5 for the TSR were attained. This configuration not only demonstrated improved self-starting attributes but also showcased heightened efficiency. Furthermore, upon comparing the proposed design configuration with previously devised hybrid VAWTs, the study demonstrated an augmentation in self-starting proficiency and overall efficiency. This serves to emphasize the potential benefits of optimizing blade numbers within a hybrid system, contributing to the on-going evolution of renewable energy technologies.

The objective of a study conducted by [20] was to delve into the intricate physics involved during the self-starting phase of a specific system. This was achieved through a

two-dimensional CFD approach. In this context, the situational simulation employed ANSYS Fluent software, where the mesh generation utilized the sliding technique, and the “Six Degrees of Freedom” (6DOF) rotational degree was enabled. The results of this research provide valuable insights into the correlation between the local absolute velocity of the blades and the instantaneous TSR during the initial and early revolutions of the motor. A noteworthy finding was that the LineAverage_1.25c technique proves to be more precise when compared to the 1-Points Average method for extracting flow dynamics around the blade. This is particularly pertinent in scenarios where flow separation and the formation of significant regions of eddies occur. Furthermore, the research delved into the behavior of dynamic stall and established the connection between the predicted angle of attack and the coefficients of lift and drag. These findings collectively contribute to an enhanced understanding of the self-starting phase’s mechanics and the aerodynamic behavior of the system under scrutiny.

For the purpose of juxtaposing studies in the existing literature, Table 1 serves as an illustrative benchmark, delineating key facets for comparison. These facets encompass:

F1–Working Mechanism of Darrieus Wind Turbine and/or Solar System: This factor delves into the operational intricacies of the Darrieus wind turbine and solar energy system, dissecting their functional synergies.

F2–Optimization Technology for Darrieus Rotor Blades: Within this parameter, the technological approaches employed for optimizing the performance of Darrieus rotor blades are examined.

F3–Geometry of Solar Panel: The geometry, configuration, and design specifics of the solar panel are appraised under this criterion.

F4–Development of Proposed Design: This factor scrutinizes the evolution and formulation of the proposed design within the context of the studied systems.

F5–Efficiency Enhancement of the System: The enhancement of system efficiency is a central consideration within this component, encompassing strategies and methodologies applied to bolster overall performance.

By dissecting these facets and presenting their nuances within [Table 1](#), a comprehensive comparison across various studies is facilitated, contributing to a more holistic comprehension of the research landscape.

3 Methodology and materials

The research method is initiated with the design of the Darrieus wind turbine rotor airfoil as the airfoil affects the self-starting capability of the rotor and its ability to generate power. In this phase, there are several parameters that must be considered such as the TSR, geometry of the rotor, drag and lift coefficient, solidity, and forces of drag and lift.

The Tip-Speed Ratio (TSR) is the ratio of the tangential speed of the tip of a wind turbine blade to the speed of the wind. If a wind turbine has a TSR of 5, it means the tip of the blade is moving five times faster than the wind speed.

The Geometry of the Rotor refers to the physical dimensions and characteristics of the wind turbine rotor, including the length and shape of the blades. A rotor with longer blades will capture more wind energy, while the shape of the blades influences aerodynamic performance.

The Drag Coefficient represents the drag force experienced by an object moving through a fluid, in this case, the wind. A low drag coefficient indicates that the rotor blades encounter less resistance, improving overall efficiency.

The Lift Coefficient measures the lift force generated by the wind turbine blades due to aerodynamic lift. A higher lift coefficient signifies increased lift force, contributing to the efficient rotation of the wind turbine.

Solidity is the ratio of the total blade area to the swept area of the rotor and provides insight into how much space the blades occupy in the rotor plane. A low solidity indicates more space between blades, potentially reducing interference and improving efficiency.

Forces of Drag and Lift represent the aerodynamic forces acting on the wind turbine blades, influencing their motion. Understanding the forces of drag and lift is crucial for optimizing blade design and overall performance in capturing wind energy.

The proposed system is then simulated with using Q-blade to understand the overall performance of the system. The airfoil of the turbine will also be simulated using the software. Further analysis will be conducted using CFD to compare the results to the results obtained from Q-blade simulations, in addition to the other parameters that is obtained from CFD analysis. [Figure 1](#) shows the isometric view of the hybrid power generator consisting of all the previously mentioned components. The battery is placed at the bottom for the stability of the hybrid power generator while also optimizing the geometrical placements of the components.



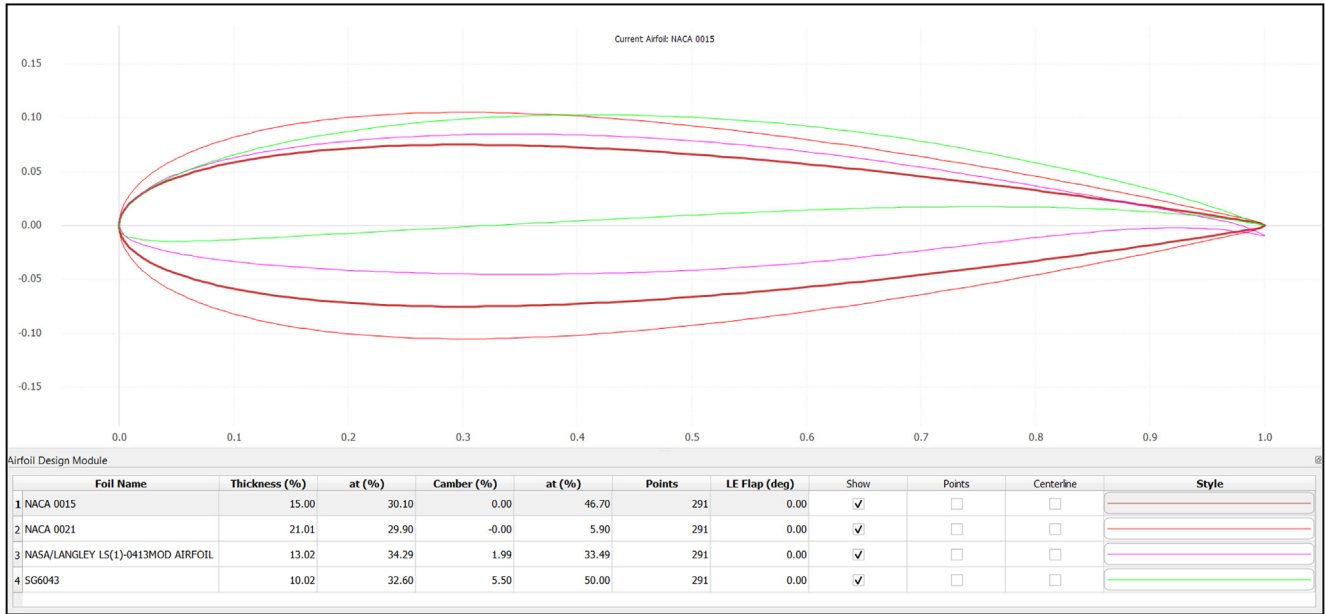
Fig. 1. Isometric drawing of the hybrid solar-wind turbine power generator.

Table 2. Geometry of the wind turbine rotor.

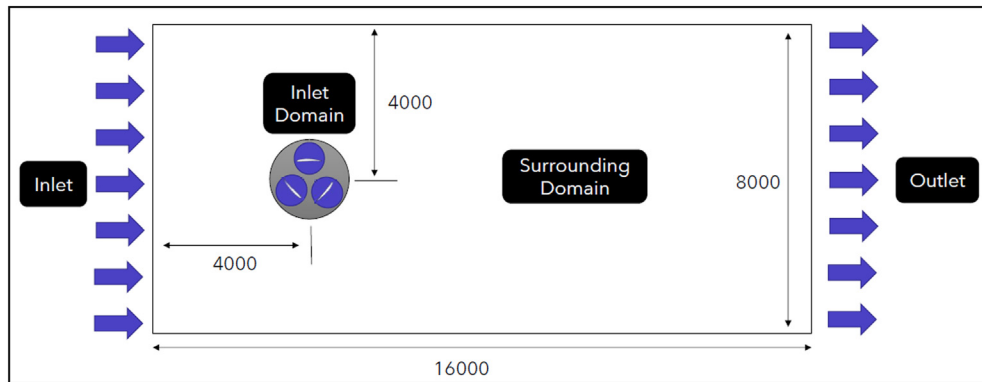
Parameter	Optimized Value	Unit
Airfoil	SG6043	–
Chord Length	0.0588	m
No. of blade	3	–
Pitch angle	–3.41	deg
Rotor diameter	0.4	m
Rotor height	0.3239	m
Solidity	0.441	–

[Table 2](#) displays the finalized geometry of the wind turbine rotor blade. The rotor is designed to have an overall diameter of 0.4 m and a rotor height of 0.3239 m. One turbine is to be used in the system. The rotor is equipped with three blades with the optimal LS (1)-0413 airfoil obtained from the optimization of the airfoil.

[Figure 2a](#) displays the view of overall view of four airfoils designed using Q-blade to propose the optimal design to be used in the hybrid solar-wind power generator. As previously mentioned, LS (1)-0413 is one of the airfoils that are being compared to other airfoils. NACA 0015 and NACA 0021 have been used as airfoils to be compared due to them being known as the conventional airfoils used. SG6046 has been determined as one of the airfoils of comparison due to the research by [\[32\]](#) that suggests the airfoil is the most effective airfoil for wind with low Reynolds number and used in a small VAWT. The research found that SG6043 obtained the largest lift to drag ratio of the airfoils compared airfoil if NACA0018, NACA0021, and LS (1)-0413.



(a)



(b)

Fig. 2. (a) Overall view of the six airfoils designed, (b) Boundary conditions of wind turbine CFD simulations.

Figure 2b illustrates the geometry to be simulated and the boundary conditions are determined to then be sent to the mesh generator. The geometry of the 2D airfoils has been drawn in ANSYS Fluent in the shape of the rotor turbine with diameter of 0.4m where the surfaces of the airfoils act as walls.

The formulations for the tip speed ratio (Eq. (1)), coefficient of moment (Eq. (2)), and coefficient of power (Eq. (3)) are as follows [32]:

$$\lambda = \frac{\omega R}{U_\infty} \quad (1)$$

$$C_m = \frac{T}{\frac{1}{2} \rho A R U_\infty^3} \quad (2)$$

$$C_p = \frac{P}{\frac{1}{2} \rho A U_\infty^3} \quad (3)$$

3.1 System components

The material selection for a hybrid solar-wind system involves considering various factors such as durability, efficiency, cost-effectiveness, and sustainability. In Malaysia, being an equatorial country, the daily average solar radiation ranges approximately from 4,000 to 5,000 Wh/m², with an annual average of 1,643 kWh/m² of received radiation. The proposed system design is illustrated in Figure 3. A summary of the materials selected for different components of the system:

- Solar Panels: A 10-Watt, Mono-crystalline Silicone is used due to its high efficiency (17%-22%), aesthetic appearance, non-hazardous to the environment, longevity, and more electricity generation.
- Mounting Structure: Aluminium is chosen as the material for the mounting structure due to its strength, durability, and corrosion resistance.



(a)



(1) Microcontroller



(2) Relay



(3) Temperature and Humidity Sensor



(4) Voltage Sensor



(5) AC to DC 5V-12V Adapter



(6) Switch (On/Off Socket)



(7) IoT Platform



(8) Battery Storage

(b)

Fig. 3. Tested system parts (a) Experimental setup, (b) Designed system materials.

- Inverter: The inverter is responsible for converting the DC power produced by the solar panels into AC power that can be used in the home. The selection of the inverter is based on efficiency, reliability, and compatibility with the solar-wind system.
- IoT Monitoring System, Microcontroller: The ESP8266 microcontroller is chosen due to its affordability, compatibility, available resources, and lower power consumption.
- Relay: A 5V-12V relay is used to control the power supply from the solar-wind system.
- Voltage Sensor: A 25V voltage sensor is used to monitor the main grid power supply.
- AC to DC 5V-12V Adapter: It serves as a power supply for the microcontroller and other components.
- Switch (On/Off Socket): It allows control of power flow to the load.
- IoT Platform, Blynk is chosen as the cloud server for the IoT system due to its open-source nature, cost-free usage, connectivity with microcontrollers via Wi-Fi, and easy-to-use graphic interface design.
- Battery Storage: Lead-acid batteries are chosen for the hybrid system due to their long lifespan, low maintenance requirements, high reliability, recyclability, low self-discharge, and efficiency at high temperatures. They are also cost-effective.

Figure 3b illustrates the designed system materials.

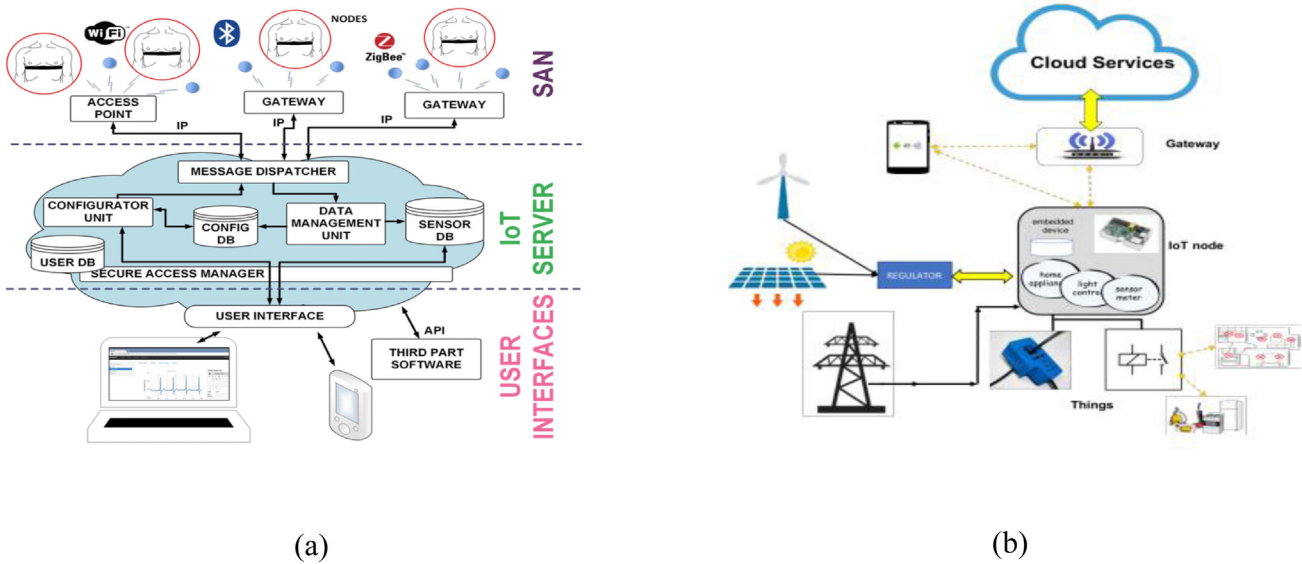


Fig. 4. (a) Block diagram of an IoT Platform, (b) IoT devices architecture.

3.2 Integration strategy

The methodology encompasses the design specifications and process for the IoT system as shown in Figure 4a. It begins with a detailed discussion of IoT principles, emphasizing the significance of understanding its functionalities for software integration. A critical aspect addressed is the proposed monitoring system design, crucial for data management and analysis, facilitating issue identification, device optimization, and system efficiency.

The IoT architecture is presented, comprising four layers: application, cloud management, network, and device. The application layer collects user data and offers smart services, while the cloud management layer centrally controls and analyses data. The network layer facilitates device connectivity, and the device layer collects data from sensing equipment and smart devices, transmitting it to the cloud.

The transmission hardware design, illustrated in Figure 4b, involves a wireless sensor network, server cloud management, and a workstation. Sensors collect data and transmit it through a Wi-Fi module, connecting with the cloud server that processes and stores the information. The workstation serves as the central control centre accessible via remote login.

The proposed approach's process flow is depicted in Figure 5a, illustrating sequential operations. The system starts with Arduino establishing an internet connection, generating an IP address. Valuable data from the hybrid system and sensors is processed by the microcontroller and efficiently transferred to the Blynk cloud server, accessible to authorized users.

The circuit design in Figure 5b incorporates two sensors controlled by the microcontroller to read data and energy from the hybrid system. The microcontroller is powered by a 5V-12V adapter, and a relay module allows remote and automatic control of the hybrid system on/off switch. The system's codes are developed in the Arduino IDE software for seamless data transfer.

3.3 Performance evaluation

The performance of the system is assessed and compared against meticulously calibrated sensor data. Calibration is conducted for the voltage and temperature sensors using a multi-meter and a thermometer, respectively, to ensure precise readings. To determine the variation between the actual and theoretical values, the percentage difference will be computed based on the calibration results obtained from the sensors. The Mean Formula will be employed to calculate the average data value, while the Standard Deviation Formula will be utilized for assessing standard deviation. It is important to note that standard deviation serves as a measure of uncertainty, representing the accuracy of the data.

The following formulas are employed for the calculations [2]:

Mean Formula

$$\text{Mean}(\mu) = \frac{V_1 + V_2 + \dots + V_n}{n} = \frac{\sum_{i=1}^n V_m}{n} \quad (4)$$

Standard Deviation Formula

$$\text{StandardDeviation}(\sigma) = \sqrt{\frac{\sum_{i=1}^n (V_i - V_m)^2}{n - 1}} \quad (5)$$

3.4 System design and analysis

This section addresses material selection and cost analysis for key components of the hybrid system, encompassing the solar module, wind turbine design, IoT cloud infrastructure, IoT programming, and software integration. This integration facilitates remote monitoring through the Blynk web and app platform, employing the NodeMCU Wi-Fi module to interface with temperature and humidity sensors, voltage sensing, and a relay module to regulate

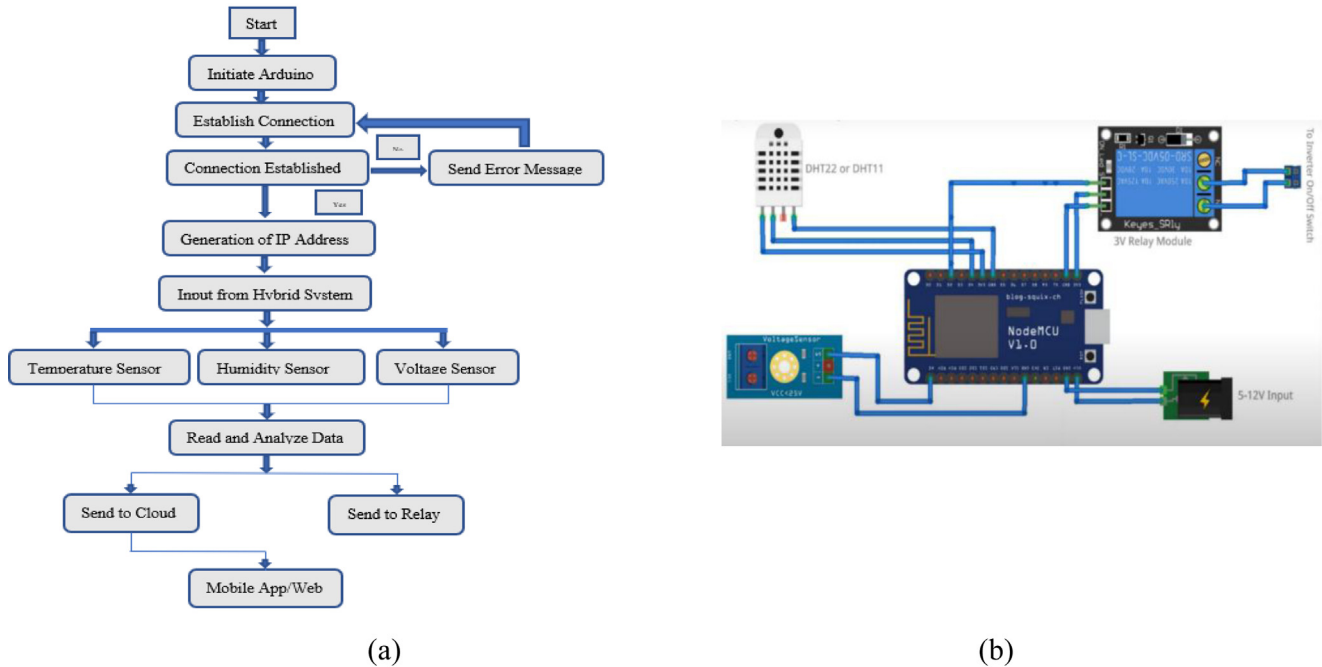


Fig. 5. (a) Process flow chart of proposed approach, (b) circuit diagram sensors & microcontroller.

power flow. The IoT system is coded utilizing the Arduino IDE platform and data transmission occurs via Wi-Fi connectivity to the NodeMCU.

This segment outlines the process of wind turbine blade design and simulation utilizing the blade element momentum theory (BEMT) through Q-blade software. The simulation entails establishing crucial design parameters, including design wind speed, rotor diameter, blade count, TSR, rotational speed, airfoil choice, and Reynolds number. The analysis with Q-blade assesses the conceptual design, allowing a comparative analysis of three distinct Horizontal Axis Wind Turbine (HAWT) blades in accordance with suggested criteria. Subsequently, the study identifies the most optimal design within this context.

Furthermore, this stage centred on formulating and executing an IoT framework for the hybrid PV solar-wind system. The Blynk platform, along with Arduino software, NodeMCU, relay module, temperature and humidity sensor, voltage sensor, and requisite components, were meticulously integrated. This integration was accompanied by a practical circuit diagram, complemented by meticulous coding to ensure the systematic surveillance of system data and the remote control of the system through the relay. In tandem with this effort, the hybrid PV solar-wind system was constructed, the IoT architecture was meticulously devised, and the Blynk platform was adeptly configured to facilitate the wireless transmission of data via Wi-Fi. The iterative blade design process was executed through the utilization of Q-blade software—an open-source wind turbine calculation tool that expedites the design of turbine blades. This is achieved by establishing chord and twist angle distributions. The Q-blade software,

rooted in the Blade Element Momentum theory, is seamlessly incorporated within an XFOIL graphical user interface.

3.4.1 Blade design mathematical model

The mathematical expressions used to calculate the data required for the blade design are defined by reference [33]. The design wind speed has been calculated using equation (6)

$$V_{design} = 1.4 \times maws \quad (6)$$

V design is the Design Wind Speed and *maws* is the *meanannualspeed* in Malaysia

$$\lambda = \Omega \times R_{rotor} / V_{design} \quad (7)$$

Where λ Tip Speed Ratio: R is blade length, Ω is the rotational speed, and V design is the design wind speed. The Local Tip Speed Ratio (λ_r) is calculated using equation (8)

$$\lambda_r = \lambda \left(\frac{r}{R} \right) \quad (8)$$

where *r* is the local radius and R is the blade length. The Rotational Speed (Ω) is obtained in equation (9)

$$\Omega = (\lambda \times V_{design}) / R \quad (9)$$

Equation (10) in the mathematical expression for the Reynolds Number (Re)

$$Re = (P \times C \times u_{rel}) / \mu \quad (10)$$

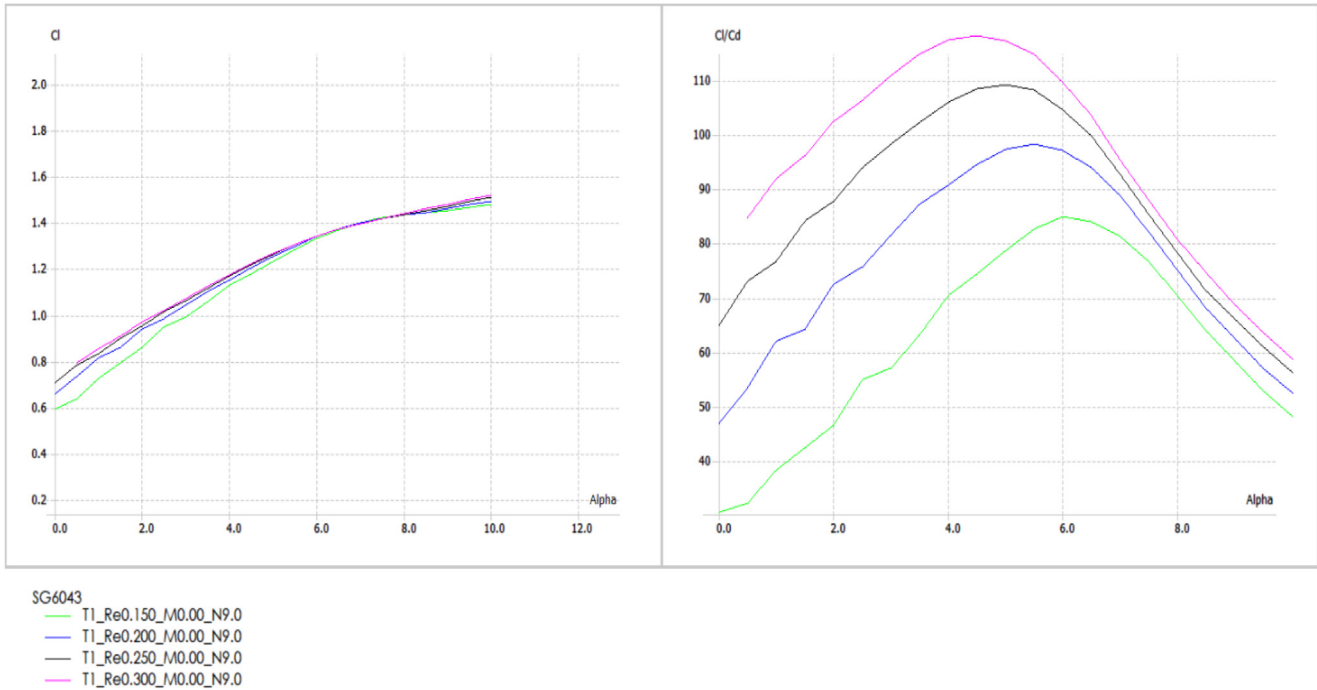


Fig. 6. Cl/Cd Max, Cl max of SG6043 of various Re.

Where ρ is the air density μ is dynamic viscosity, C is the chord length and u_{rel} is the relative wind speed.

The Initial Angle of the Relative Wind (pi) is expressed in equation (11)

$$pi = 90^\circ - \left(\frac{2}{3}\right) \times 90 - \left(\frac{2}{3}\right) \tan^{-1}\left(\frac{1}{\lambda_r}\right) \quad (11)$$

Equation (12) is used to calculate the Chord Length (C_r) and Lift coefficient (Cl)

$$C_r = (8\pi \times \sin\phi_i)/(3 \times N \times Cl \times \lambda_r) \quad (12)$$

Where N is the number of blades, and ϕ is the optimum relative wind angle. The Local Twist Angle (θ_r) is obtained by equation (13)

$$\theta_r = \Phi_i - \alpha_{opt} - \beta \quad (13)$$

Where: a_{opt} is the optimal angle of attack, and β is the pitch angle. The mechanical power extracted by the WT is calculated by equation (14)

$$Pm = 0.5 \times \rho \times \pi \times v^3 \times R^2 \times Cp(\lambda, \beta) \quad (14)$$

Where Cp is the rotor power coefficient (the turbine's maximum efficiency), and V is the available wind speed.

Enhancing rotor blade performance hinges upon the judicious selection of airfoil shapes that yield heightened lift and lift-to-drag ratios. The pursuit of airfoils with a high lift-to-drag ratio proves especially advantageous for compact rotor dimensions, as they engender substantial torque generation and manifest optimal responsiveness at lower wind speeds, culminating in efficient power generation. Furthermore, the zenith of rotor blade efficacy is

reached in conditions of gentle winds. Under such circumstances, the optimization of Reynolds numbers, as defined by equation (10), harmonizes with other parameters appraised by the BEMT. Given that low Reynolds numbers arise from the operation of diminutive rotor Wind Turbines (WTs) within the realm of low wind velocities, securing a high-performance rotor in this context necessitates airfoils boasting elevated lift and lift-to-drag ratios at low Reynolds numbers and angles of attack. To materialize this, the blade span, encompassing a radius of 0.7 m, is segmented into ten equal-length elements. Reynolds numbers of 1.5×10^5 , 2.0×10^5 , 2.5×10^5 , and 3.0×10^5 are contemplated. Airfoil data files are subsequently transposed into Q-blade software for analysis, delving into lift and drag coefficients at varying Reynolds numbers. For each chosen airfoil and Reynolds number, the pinnacle points of maximum lift and minimum drag coefficients, engendering the most favourable glide ratio, are pinpointed. The associated angles of attack that yield these optima are also discerned, as depicted in Figure 6 as an example. Referring to Table 3, it becomes evident that the SG6043 airfoil has achieved the pinnacle lift-to-drag ratio, reaching a remarkable value of 118 at a Re of 3.0×10^5 and an angle of attack of 4.5 degrees. In contrast, the NACA 4412 airfoil attains its highest lift-to-drag ratio, reaching 91.3, under the conditions of a Re of 3.0×10^5 and an angle of attack of 7.5 degrees. This analysis leads to the conclusion that the well-suited airfoil and Re combination are the SG6043 airfoil and a Re of 3.0×10^5 , respectively.

3.4.2 TSR and rotational speed

One pivotal parameter in blade design influencing the initiation speed of the rotor is the TSR. With an emphasis on rapidly achieving the required torque for startup and attaining optimal power capture within a low wind speed

Table 3. Selected Airfoils data at $Re\ 3.0 \times 10^5$.

	3.0×10^5			
Airfoils	cl/cd max	cl max	cd min	α opt
SD2030	89.1	0.695	0.0079	3.5
NACA4412	91.3	1.25	0.0137	7.5
SG6043	118	1.22	0.0103	4.5

domain, the TSR values of 4, 5, and 6 were carefully chosen for incorporation into the design. Subsequently, equation (9) was employed to calculate Ω corresponding to each designated TSR.

Referencing Table 4, the rotational speed values mark the juncture at which the rotor blade garners its peak power output, synchronized with the design wind speed and the optimal TSR setting. The parameters essential for configuring the blade design within the Q-blade software are accurately computed through the application of the design equation for TSR values of 4, 5, and 6, respectively.

The analysis reveals that the pinnacle of optimization emerges at a TSR of 6, as illustrated in Figure 7a. Additionally, Figure 7b elucidates that the optimal configuration achieved at a TSR of 6 yields the highest power coefficient in alignment with the desired outcome.

3.4.3 Cost analysis

To ascertain the feasibility of adopting this technology, a comprehensive cost analysis will be undertaken. This study aims to meticulously assess both the expenditures and benefits inherent to this project. The anticipated material costs for implementing this hybrid renewable energy technology are detailed in Table 5. The findings indicate that the system cost remains favourable in comparison to analogous systems documented in the existing literature.

4 Results and discussion

4.1 Calibration of sensors result

To calibrate the sensors, a comparison will be made between theoretical values and actual values. The actual data was collected through an 8 h monitoring period, spanning from 9:00 AM to 5:00 PM. The theoretical data, on the other hand, were acquired by employing a multimeter and a thermometer. Subsequently, the collected data was consolidated and summarized using the mean and standard deviation formulas. The calculation process for determining the mean and standard deviation of each sensor is elucidated in the Tables 6 and 7.

By calculating the percentage difference from standard measuring instrument ($\mu \pm 1\sigma$ %) between the Mean value and the Standard Deviation value, the result of the Standard Deviation value will show how far or how close the dispersion of data from mean value. It is found that μ for voltage and temperature are 10.0978, and 28.944, while σ for voltage and temperature are 0.0180, and 0.5003, respectively.

Table 4. Rotational speed of varying TSR.

	Design wind speed = 4.0 m/s		
Chosen TSR and rotational speed for turbine design			
TSR	4	5	6
Ω (rad/s)	24.69	30.86	37.03

4.2 Hybrid system results

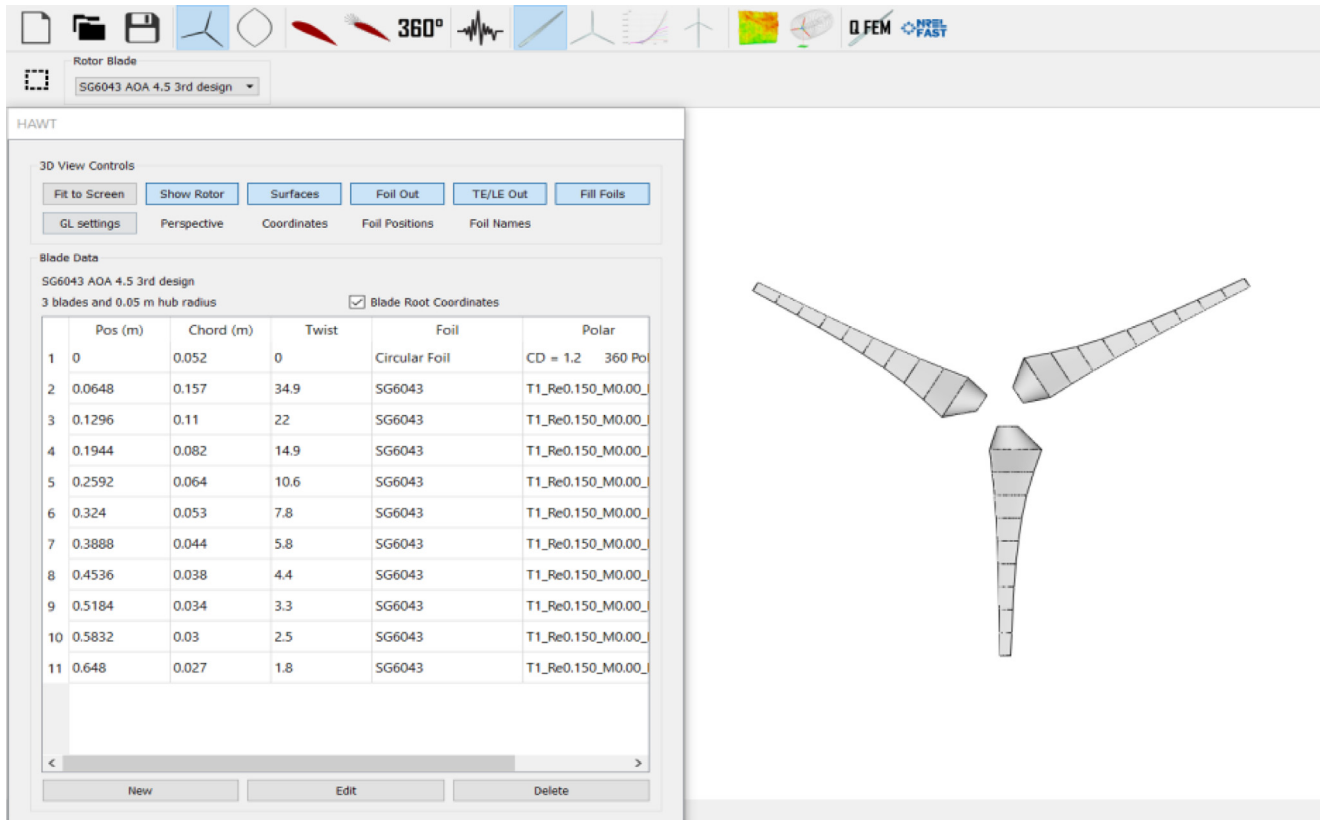
Based on predicted winds in Kajang, Malaysia, between 17th February and 24th March 2023, Figure 8a illustrates the results of theoretical computations. According to the theoretical calculations, the overall efficiency rating for both the wind turbine and gearbox/generator systems is 31.5%. In Figure 8b, the coefficient of moment is plotted against the TSR for wind velocities of 2 m/s, 3 m/s, and 4 m/s. At a wind speed of 3 m/s, the C_m graph shows the ideal pattern, in which C_m ascends to a peak and then descends. This trend, on the other hand, is not valid for wind speeds of 2 m/s and 4 m/s, as their respective graphs show fluctuating increments and decrements.

At a wind velocity of 2 m/s and a TSR of 2.4, the pinnacle of C_m stands out as the singular point where a positive value is reached, specifically at 0.0288. Remarkably, this marks the highest C_m value across all simulated scenarios. Conversely, the minimum coefficient of moment, registering at -0.0899 , transpires at a TSR of 2.2, establishing the lowest value of C_m within the entire dataset.

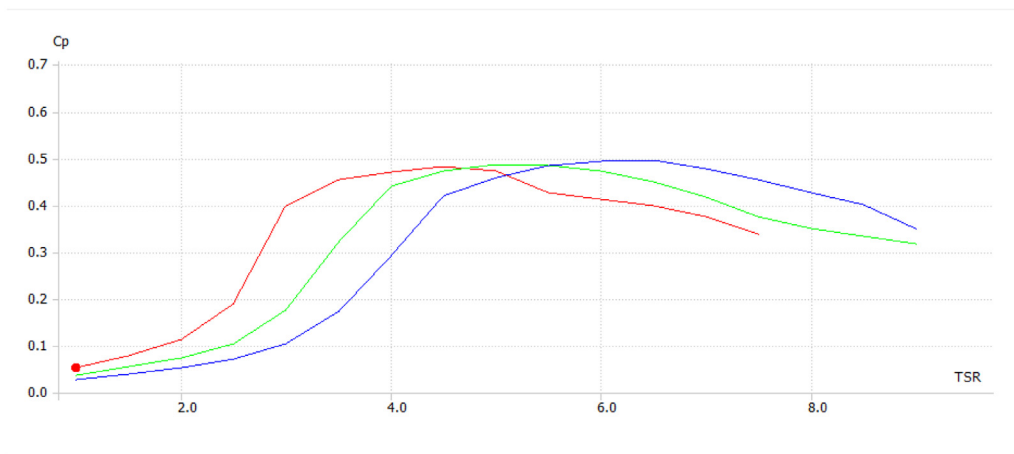
Upon analysing the wind velocity of 4 m/s, the zenith coefficient of moment emerges at 0.0269, aligning with a TSR of 2.2. In contrast, the nadir value of C_m presents itself at -0.0282 for a TSR of 3.0. Furthermore, for wind speeds of 4 m/s, positive C_m values are observed at TSR 2.8, specifically at 0.0047. Similarly, for wind velocities at 3 m/s, positive C_m values are discernible at TSRs of 2.4 and 2.6, registering at 0.0184 and 0.0105, respectively. The lowest C_m value recorded within this wind speed category is a substantial -0.0249 , occurring at a TSR of 2.2.

A theoretical wind turbine in Kajang, Malaysia generates electrical power at high wind speeds as shown in Figure 9a. According to the graph, the highest expected electrical power generation occurred on the 14th of March 2023 at 0.88 kW, while the lowest was on the 20th of February at 0.06 kW. There is a steady increase in electrical power generation from the 20th to the 3rd of March. In spite of this, the results may vary due to the cut-in wind speed of wind turbines, which is generally 4 m/s, but the forecasted wind speeds are not more than 3.06 m/s. As a result, the wind turbine will generate electricity on an hourly basis.

From the moment obtained from the CFD simulations, the power is then able to be calculated to determine the ability of the turbine. Table 8 comprises of the calculated power of the turbine for wind speeds of 2 m/s, 3 m/s and 4 m/s for TSR of 1, 2, 2.2, 2.4, 2.6, 2.8, and 3.0. From the table above the coefficients of power were also calculated to



(a)



SG6043 @ AOA 4.5 (TSR:4)
 — SG6043 @ AOA 4.5 (TSR:4) Simulation

SG6043 @ AOA 4.5 (TSR:5)
 — SG6043 @ AOA 4.5 (TSR:5) Simulation

SG6043 @ AOA 4.5 (TSR:6)
 — SG6043 @ AOA 4.5 (TSR:6) Simulation

(b)

Fig. 7. (a) Optimal rotor design, (b) Power coefficient of the designed rotors.

Table 5. The estimated cost of materials in the system.

Parts	Price/unit (RM)	Quantity	Total (RM)
10W PV solar panel mono-crystalline silicon	75.80	2	151.60
Microcontroller NodeMCU ESP8266	27.80	1	27.80
Temperature/Humidity sensor – DHT22	19.80	1	19.80
Relay Module	8.40	1	8.40
Solder Cable	11.22	1	11.22
DC to AC Inverter	173.90	1	173.90
Jumper Wire for NodeMCU	3.60	3	10.80
Total Cost (RM)			403.52

Table 6. Voltage sensor (Theoretical vs. Experimental).

Monitoring Time	V_i , Voltage (Multi-meter)	Voltage (Sensor, V)	Average, V_m	$(V_i - V_m)^2$
9:00 AM	7.14	7.24	7.19	$(7.14 - 7.19)^2 = 0.0025$
10:00 AM	10.91	10.93	10.92	$(10.91 - 10.92)^2 = 0.0001$
11:00 AM	10.90	10.93	10.915	$(10.90 - 10.915)^2 = 2.5 \times 10^{-5}$
12:00 PM	10.94	10.95	10.945	$(10.94 - 10.945)^2 = 2.5 \times 10^{-5}$
1:00 PM	11.55	11.54	11.545	$(11.55 - 11.545)^2 = 2.5 \times 10^{-5}$
2:00 PM	12.25	12.26	12.255	$(12.25 - 12.255)^2 = 2.5 \times 10^{-5}$
3:00 PM	10.95	10.95	10.95	$(10.95 - 10.95)^2 = 0$
4:00 PM	9.42	9.42	9.42	$(9.42 - 9.42)^2 = 0$
5:00 PM	6.74	6.74	6.74	$(6.74 - 6.74)^2 = 0$
Sum			90.88	0.0026

Table 7. Temperature sensor (Theoretical vs. Experimental).

Monitoring Time	T_i , Temperature (Thermometer)	Temperature (Sensor)	Average, T_m	
9:00 AM	23.9	24	23.95	$(23.9 - 23.95)^2 = 0.0025$
10:00 AM	24.1	24	24.05	$(24.1 - 24.05)^2 = 0.0025$
11:00 AM	27.0	27	27	$(27.0 - 27)^2 = 0$
12:00 PM	31.0	29	30	$(31.0 - 30)^2 = 1$
1:00 PM	30.0	31	30.5	$(30.0 - 30.5)^2 = 0.25$
2:00 PM	32.0	33	32.5	$(32.0 - 32.5)^2 = 0.25$
3:00 PM	32.0	32	32	$(32.0 - 32)^2 = 0$
4:00 PM	31.0	31	31	$(31.0 - 31)^2 = 0$
5:00 PM	29.0	30	29.5	$(29.0 - 29.5)^2 = 0.25$
Sum			260.5	2.0025

determine the efficiency of the turbine at the specified environments. Hence, the graph for power and coefficients of power were developed below.

Figure 9b displays the graph of coefficient of power against the TSR for wind speeds of 2 m/s, 3 m/s and 4 m/s. Identical to the previous graph, the graph shows and increasing trend until it reaches the peak at TSR of 2.2 and continues to consistently decrease until TSR is 3. The coefficient of power is also described as the efficiency of the turbine as it represents the ratio of power out to the power in. These coefficients must be below the Betz limit of 0.5926 which is the ideal condition of a wind turbine. In contrast to

the power produced which indicated that the largest power produced by as much as 2.3779 W at 4 m/s and TSR of 2.2, the most efficient condition was obtained at wind speed of 3 m/s at TSR of 2.2 with the coefficient of power of 0.3345. The coefficient of power measured at TSR of 2.2 for both wind speeds of 2 m/s, and 4 m/s was by as much as 0.1641 and 0.1588 respectively.

Figure 10a shows how the wind flow creates drag on the wind turbine blades due to large areas of high velocity. The display of various speeds of wind within the area inside of the blades shows that the wind is not being fully utilised, thus strengthening the simulated results obtained from the

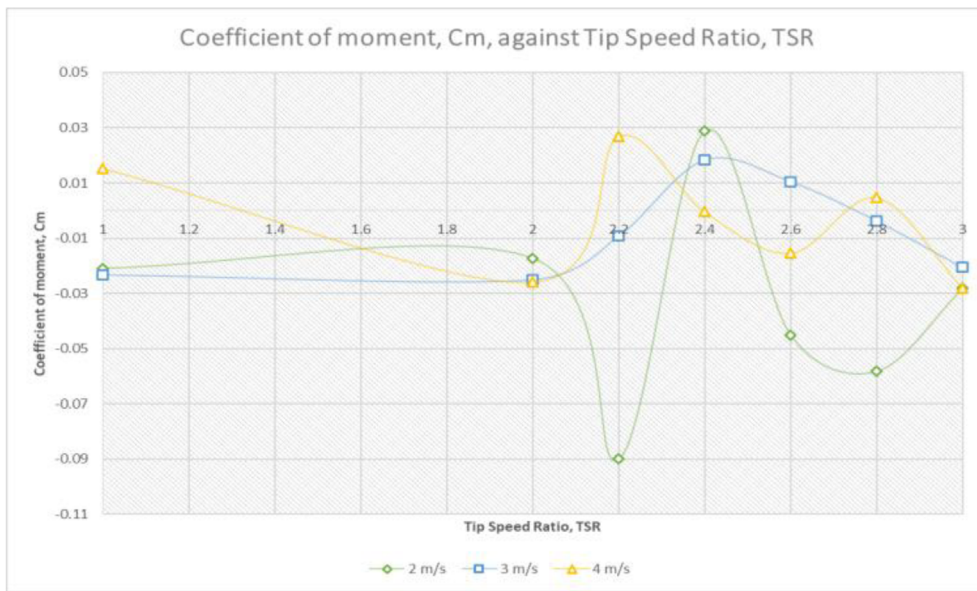
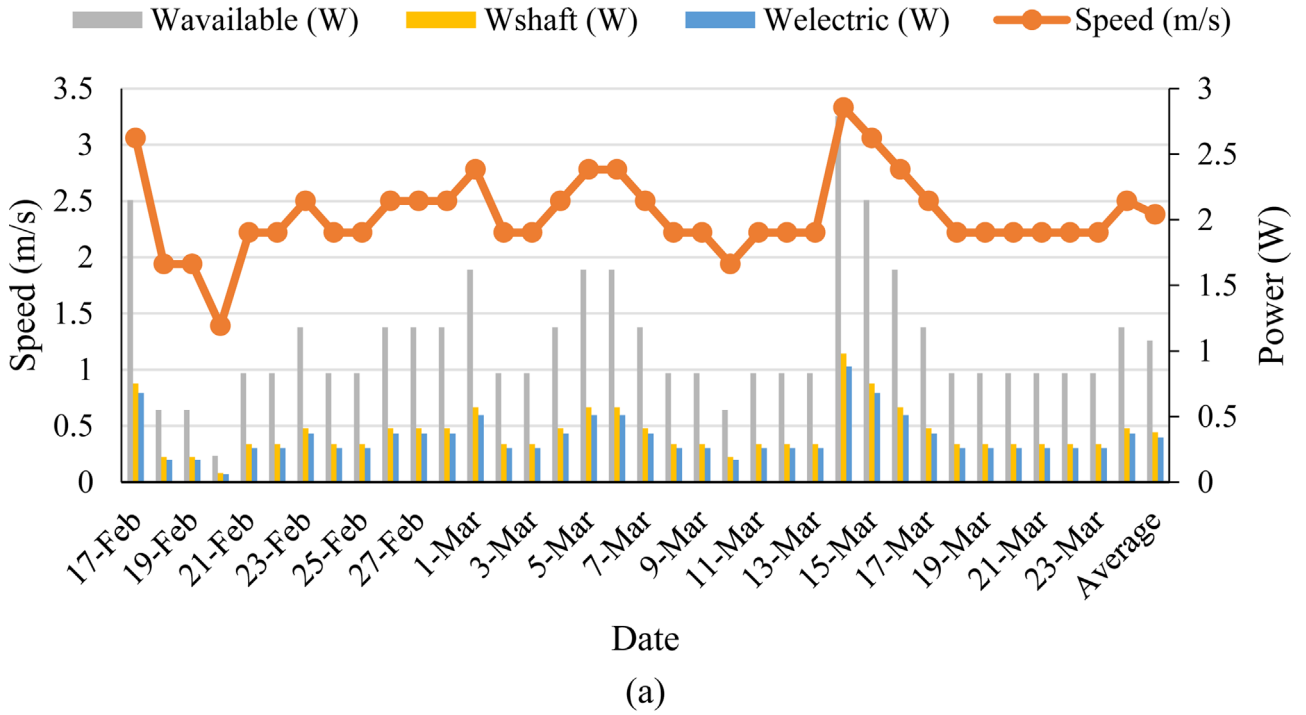
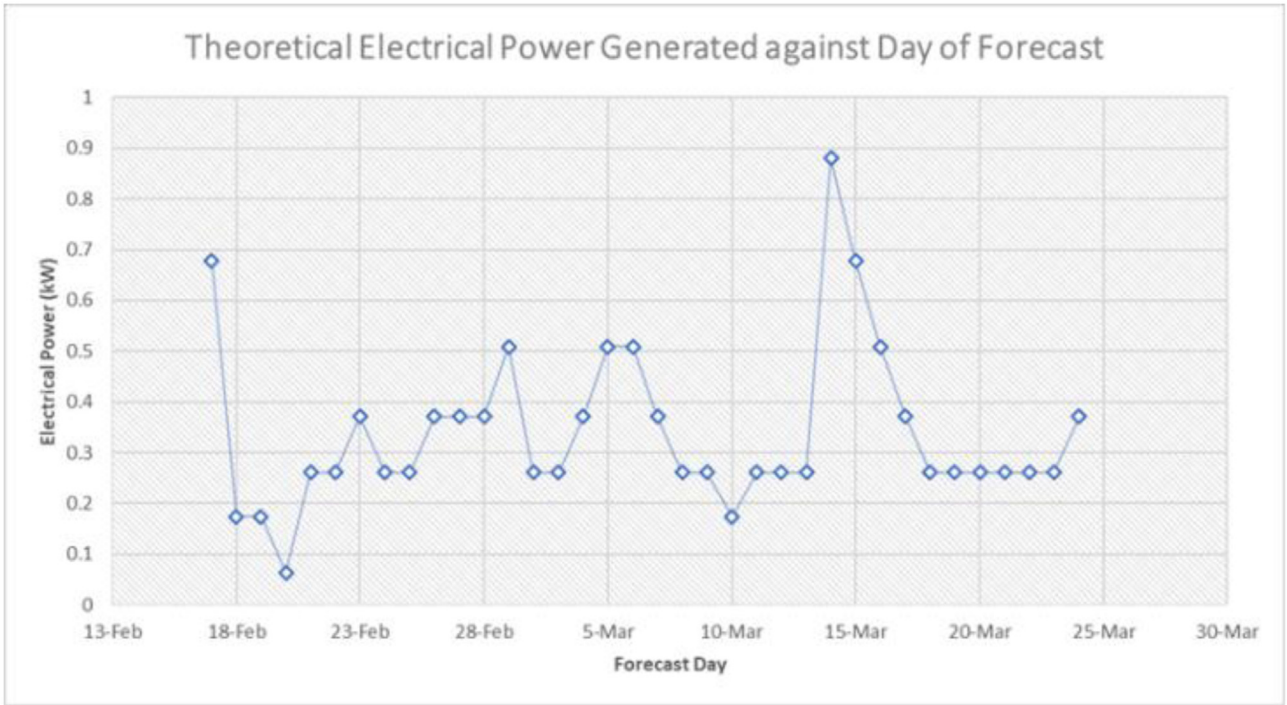
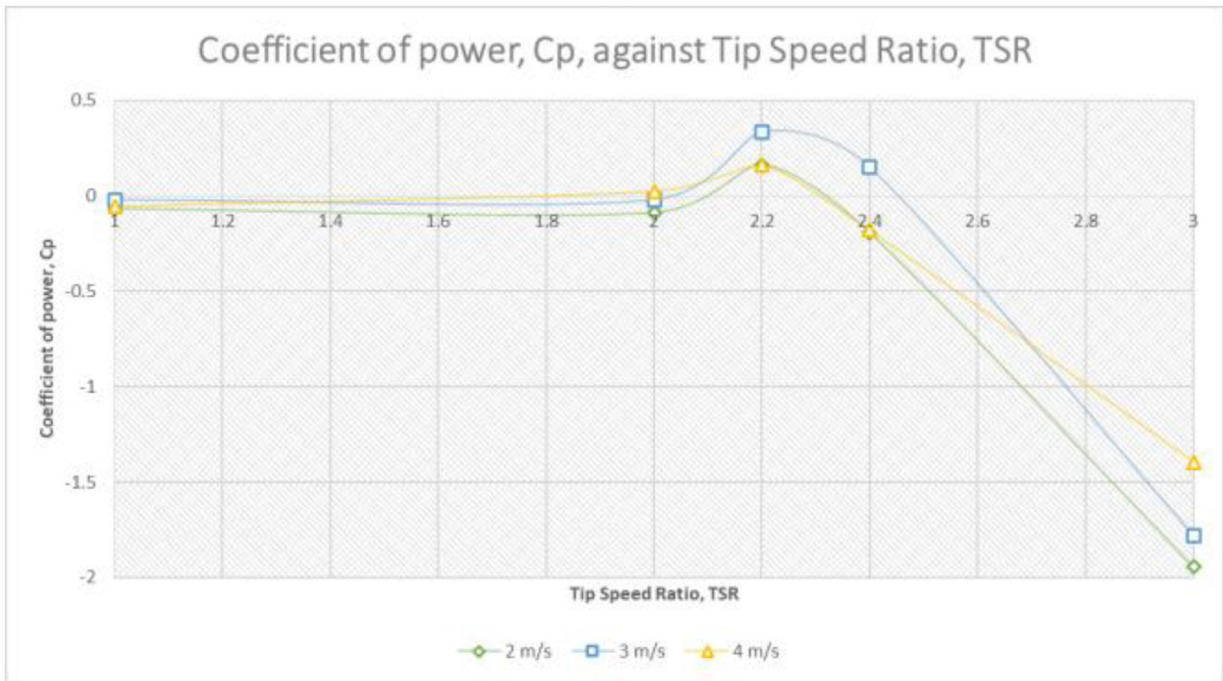


Fig. 8. (a) Predicted power generation from WT, (b) C_m against TSR at wind speeds of 2 m/s, 3m/s, and 4m/s.



(a)



(b)

Fig. 9. (a) Theoretical power generation over the forecasted days, (b) Cp against TSR for wind speeds of 2 m/s, 3 m/s, and 4 m/s.

Table 8. Moment and coefficient of power at different TSR and wind speed.

Tip Speed Ratio	Wind speed (m/s)	Power(W)		Coefficient of power, Cp			
		2	3	4	2	3	4
1		-0.0782	0.4397	0.9193	0.0418	0.0696	0.0614
2		-0.1296	-0.9451	-3.0996	-0.0692	-0.1496	-0.2070
2.2		-0.7406	-0.7559	3.5429	-0.3956	-0.0595	0.2366
2.4		0.2587	0.8359	0.0663	0.1382	0.1323	-0.0044
2.6		-0.4400	0.5168	-2.4068	-0.2350	0.0818	-0.1607
2.8		-0.6090	-0.2002	0.7895	-0.3258	-0.0317	0.0527
3.0		-0.3160	-1.1711	-5.0663	-0.1688	-0.1854	-0.3383

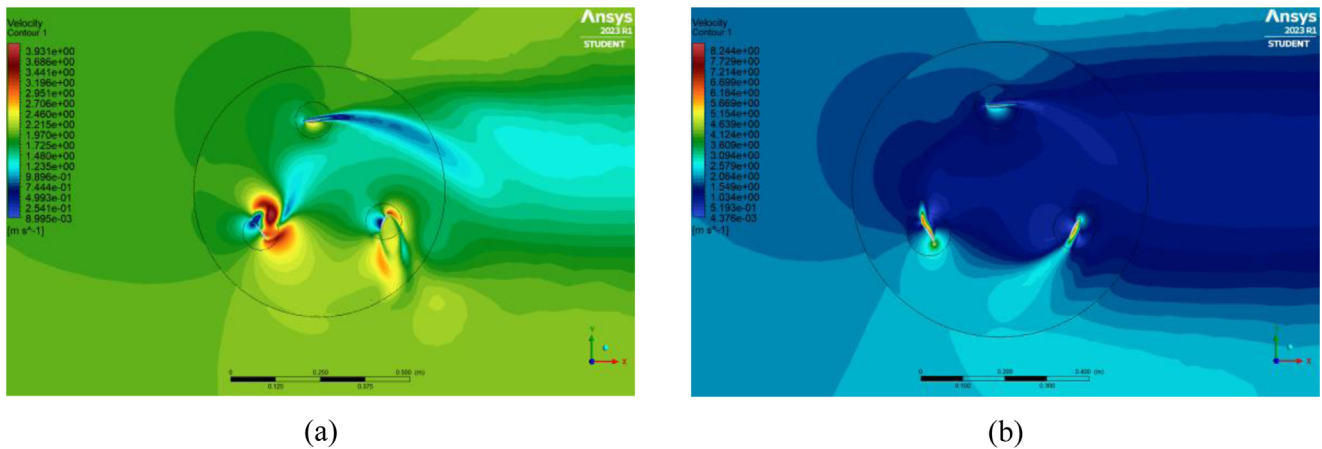


Fig. 10. Velocity Contours across turbine blades at wind speed 2 m/s at a) TSR = 1, b) TSR = 2.2.

Table 9. Data calibration of each sensor.

Sensor Type	Percentage difference from standard measuring instrument ($\mu \pm 1\sigma$ %)
Voltage	10.0978 \pm 0.0180 %
Temperature	28.9444 \pm 0.5003 %

simulations previously. It is also evident from the long trail ends of the wind exiting the blade at a TSR of 1, which is another indication of poor performance. Changes in wind speed increase the pressure differences that enhance drag development and adversely affect the performance of wind turbines.

A comparison of Figure 10b shows there are fewer wind velocity contours within the turbine blades because they are able to better utilize the energy within the air at TSR's of 2 and 2.2. Compared to Figures 10a and b displays a larger area of higher velocity. As a result, a Darrieus wind turbine requires less lift force to operate because of the increased drag experienced by the blade. Similarly, the coefficients calculated from simulation results are in agreement with the results.

• *Wind turbine rotor*

Rotors were developed based on the proposed design (refer to Tab. 2). The blades were developed using 3D orienting with the material of PLA as it is most suitable for the sharp edges of the airfoil geometry. Acrylic rods were used for the shaft and connecting blade-to-shaft rods.

• *Solar panels and charge controllers*

Monocrystalline panels were used at 10W each. The solar panels were mounted at the top of the hybrid power system at an angle of 30°. Two charge controllers were used, wind turbine charge controller and solar PV charge controller, where the positive terminals of the charge controllers were connected to diodes to prevent backflow.

• *Inverter and battery*

Inverter was used to draw the DC power from the battery to AC power for the loads, which in this study uses a 20W spotlight. Battery used was a sealed lead acid battery at 12V and 18 Ah.

The percentage difference values presented in Table 9 represent the summarized results of sensor calibration, specifically focusing on the Mean and Standard Deviation ($\mu \pm 1\sigma$ %). The σ signifies the extent of dispersion between the data points and the μ , highlighting the proximity or divergence of the data.

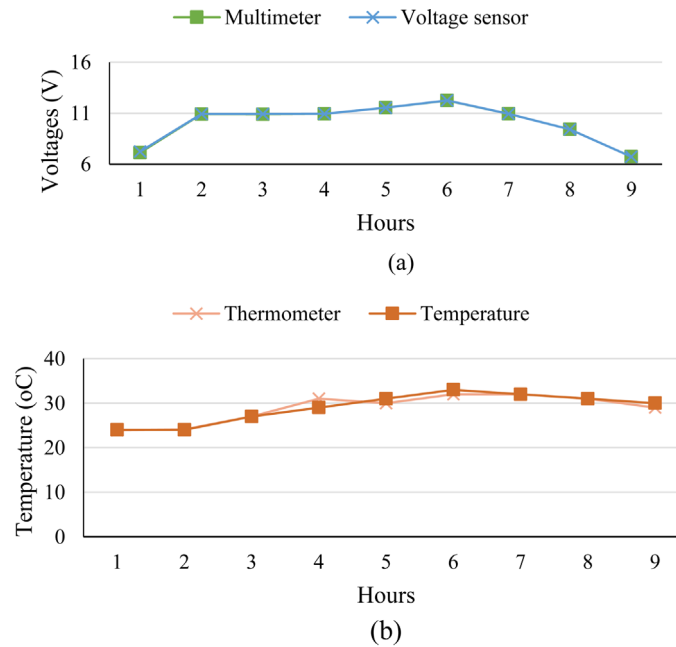


Fig. 11. Measured system (a) voltage, (b) temperature.

It can be observed that the σ values are smaller than their respective means, indicating minimal deviation from the mean. The average accuracy of all sensors was recorded at 98.59%, signifying their optimal performance and dependable data acquisition. Consequently, this outcome successfully fulfils the study's objective, which is the validation of the system's functionality. Figure 11a illustrate the dispersion of data, encompassing all tabulated information.

Based on Figure 11 it is evident that the data exhibits minimal dispersion. Despite occasional fluctuations in readings, the sensors demonstrate a remarkable level of accuracy. As a result, the validation of the system is confirmed.

The relay module, an integral part of the system, is also examined to validate its functionality. Testing involves activating and deactivating a light bulb to confirm the relay's capability to control the switch wirelessly. Additionally, the relay is found to be capable of activating the power source from the hybrid PV solar-wind system in case of a disruption in the main grid power supply.

The relay control functionality of the IoT system is extensively tested and validated as shown in Figure 12. It is confirmed that the relay effectively controls the on and off switching of the hybrid solar-wind system wirelessly and automatically, as intended. The relay's successful response to the NodeMCU signals verifies its functionality and contributes to the overall success of the IoT system for hybrid energy management.

Furthermore, the IoT technology employed in the hybrid system provides flexible monitoring mechanisms remotely through internet web connections. Users are able

to monitor voltage, temperature, and humidity remotely and control the system on/off functionality. The system's affordability, convenience, and efficiency are highlighted.

User-friendly graphical user interfaces (GUIs) are developed using the BLYNK application for data monitoring as shown in Figure 13a. The BLYNK application allows users to choose and display the desired data, such as humidity, temperature, and voltage. A web dashboard on the BLYNK website (see Fig. 13b) is also designed for administrative and management purposes, enabling data display and system control via a computer.

The monitoring system devices showcase seamless data transmission to the cloud application and website. The system's stability is ensured through a synchronized time call interval of 1 s across all sensors. This prevents potential crashes or interruptions in the system's operation, further validating its reliability.

4.3 Comparison with similar works from literature

Reviewing several publications that focused on hybrid systems combining two PV systems and a wind turbine, it has been found that all references praised the use of these systems, which complement one another and make electricity production more reliable as illustrated in Table 10. In the researchers' study, they used a variety of wind turbines that each had advantages and disadvantages, but all needed more study to generate energy at low wind speeds of 2 m/s or less. Solar photovoltaics and hybrid wind energy systems produce far fewer emissions than fossil fuel-based electricity, according to studies.

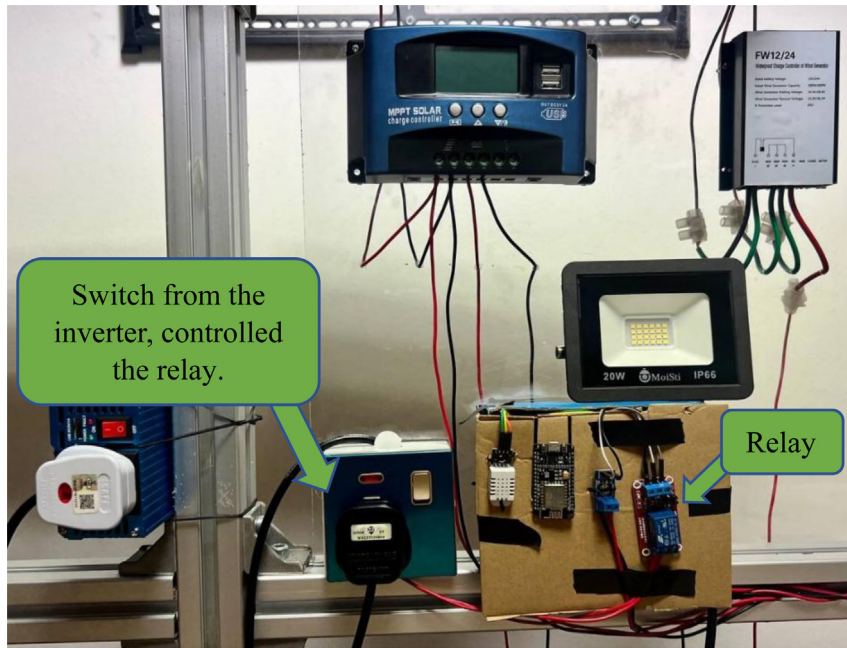
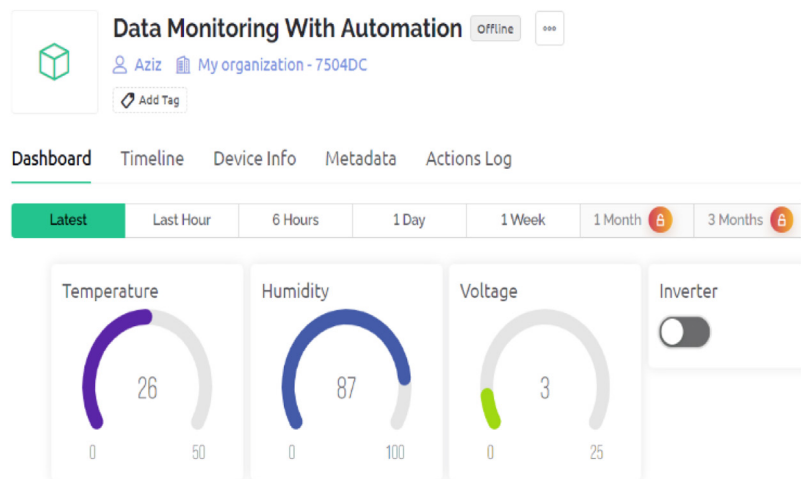


Fig. 12. The relay module connection.



(a)



(b)

Fig. 13. Data Monitoring GUI in BLYNK (a) application, (b) web dashboard.

Table 10. Comparison between the recent study and others from literature.

References	Year	Location	Solar system type	Wind turbine type	Critical findings
Eltayeb et al. [34]	2023	India	Solar panel	horizontal axis	A tree is an artificial structure that resembles a natural tree, and solar modules and wind turbines are installed on top of its branches. There is a possibility of generating 3 kilowatts of power from this system, which consists of 2 kilowatts of solar energy and 1 kilowatt of wind energy.
Sarash et al. [35]	2023	India	Single axis solar tracking	Horizontal wind turbine	The solar-wind hybrid power generation system can generate electricity continuously to meet load demands. Hybrid systems can overcome the disadvantages imposed by adverse weather conditions. Due to climatic conditions, solar energy conversion efficiency varies. In the absence of steady wind speed, wind energy cannot produce stable electricity. Hybrid power generation utilizing renewable energy is therefore more efficient in providing a stable and balanced supply of electricity.
Manusmare et al. [36]	2023	India	Monocrystalline PV panels	Vertical and horizontal turbines	The combined use of wind and solar power generation is used to model hybrid renewable energy systems. Energy can be provided continuously by the proposed hybrid system. Without disturbing the natural balance, electricity will be produced at a reasonable cost.
Muchiri et al. [37]	2023	Kenya	Monocrystalline PV panels	Vertical turbine	In the eastern region of Kenya, wind and solar resources can be integrated into hybrid energy systems. An average wind speed of 3.0 m/s was observed with a wind energy density of 17 watts/m ² . PV systems with a maximum installed capacity of 1 kilowatt will receive 2130 kWh of solar insolation per m ² on an annual basis, and 5.8 kWh per m ² on a daily basis.
Sakti et al. [38]	2023	Indonesia	Polycrystalline PV panels	Horizontal turbine	Malahing Village – Indonesia has a potential wind speed of 3.58 m/s and a potential solar radiation of 4.63 kW/m ² . Simulated results suggest the best configuration for 231 kWh/day is a 16.1 kW photovoltaic system, a 5.1 kW wind turbine, a 16.3 kW inverter, and 220 kWh of storage. A solar panel system produces 22,276 kWh of electricity per year. A total of 70,446 kWh/year are generated by the wind turbine

Table 10. (continued).

References	Year	Location	Solar system type	Wind turbine type	Critical findings
Charpota and Sharma [39]	2023	India	Polycrystalline PV panels	Horizontal turbine	<p>electrical system. Wind turbines provide 76% of the system's electricity, while solar panels provide 24%.</p> <p>A variety of renewable energy sources was used in this study to maintain voltage management and voltage stability of the entire microgrid system through the use of power electronics. These power quality problems can be fixed or at least reduced by the proposed hybrid system. In this microgrid, solar and wind power generation can fluctuate irregularly, and the energy storage system can serve as a backup power source.</p>
Recent Study	2023	Malaysia	Monocrystalline PV panels	Darrieus wind turbine	<p>An energy generation system that combines solar and wind power was developed in this study. A number of improvements were suggested to the blade shape using the Q-blade program in the study. According to the results of the study, a maximum of 0.88 kilowatts of electricity can be generated. The increased drag that is exposed to the blades of Darrieus wind turbines also reduces the required lift to operate them.</p>

5 Conclusion

In conclusion, this study presents a comprehensive approach to design and monitoring hybrid PV solar-wind systems via an IoT-based monitoring system. The proposed design seamlessly integrates sensors, micro-controllers, relay modules, and cloud servers, enabling efficient data collection, management, analysis, and remote control. The calibration process substantiates the system's reliability and precision, enabling real-time data acquisition and remote management via smartphones or computers.

The incorporation of IoT technology elevates the system's functionality and user-friendliness, thereby contributing to sustainable energy practices and resource management. This design offers a robust and effective solution for monitoring renewable energy systems, ensuring accurate measurement of system parameters and optimization potential.

Based on theoretical results, the highest electrical power generation was 0.88 kW on March 14, 2023, and the lowest power generation was 0.06 kW on February 20, 2023. As a result of the increased drag that the blades are exposed to, the Darius wind turbine requires less lift to rotate. In addition, the experimental and theoretical results converged well, meaning that the assumptions were reasonable. In addition to driving the advancement of renewable energy technologies, this research paves the way for future inquiries into improving hybrid wind-solar PV system efficiency and capabilities.

While this research has contributed significantly to the design and monitoring of hybrid PV solar-wind systems through an IoT-based approach, it is essential to acknowledge certain limitations. The theoretical assumptions made during the study, while validated by the convergence of experimental and theoretical results, pose a potential constraint. Furthermore, the research primarily focuses on system monitoring and optimization, leaving room for future investigations into external factors that may impact system performance. Moving forward, future research could delve into a more comprehensive analysis of these external factors, providing a nuanced understanding of real-world challenges.

Funding

Tenaga Nasional Berhad (TNB) and UNITEN provided support for this project through the DLTK GRANT 2023, with the project code 20238015DLTK.

Conflict of Interest

The author(s) declare that they have no conflict of interest.

Author contribution statement

All the researchers were worked equally. Each of them helped in the writing of this paper.

The authors would like to express gratitude to power generation unit, institute of power engineering, Universiti Tenaga Nasional (UNITEN) and Tenaga Nasional Berhad (TNB) for providing research grant to carry out this research.

References

1. M. Erdiwansyah, R. Mamat, M.S.M. Sani, F. Khoerunnisa, A. Kadarohman, Target and demand for renewable energy across 10 ASEAN countries by 2040, *Electr. J.* **32**, 106670 (2019)
2. A.H. Al-Waeli, H.A. Kazem, M.T. Chaichan, K. Sopian, *Photovoltaic/thermal (PV/T) systems: principles, design, and applications* (Springer Nature, 2019)
3. D. Derome, H. Razali, A. Fazlizan, A. Jedi, Distribution cycle of wind speed: a case study in the Southern Part of Malaysia, in: *IOP Conference Series: Materials Science and Engineering*, 2023, February, IOP Publishing, Vol. 1278, No. 1, p. 012010
4. K. Tantichukiad, A. Yahya, A. Mohd Mustafah, A.S. Mohd Rafe, A.S. Mat Su, Design evaluation reviews on the savonius, darrieus, and combined savonius-darrieus turbines, *Proc. Inst. Mech. Eng., Part A: J. Power Energ.* 09576509231163965 (2023)
5. B. Kirke, A. Abdolahifar, Flexible blades to improve Darrieus turbine performance and reduce cost, *Energy Sustain. Dev.* **73**, 54–65 (2023)
6. B. Al, A. Said, H.A. Kazem, A.H. Al-Badi, M.F. Khan, A review of optimum sizing of hybrid PV-wind renewable energy systems in Oman, *Renew. Sust. Energ. Rev.* **53**, 185–193 (2016)
7. H.A. Kazem, A.H. Al-Waeli, M.T. Chaichan, A.S. Al-Mamari, A.H. Al-Kabi, Design, measurement and evaluation of photovoltaic pumping system for rural areas in Oman, *Environ. Dev. Sustain.* **19**, 1041–1053 (2017)
8. A.H. Al-Waeli, H.A. Kazem, M.T. Chaichan, K. Sopian, A review of photovoltaic thermal systems: Achievements and applications, *Int. J. Energ. Res.* **45**, 1269–1308 (2021)
9. A. Khan, N. Javaid, Jaya learning-based optimization for optimal sizing of stand-alone photovoltaic, wind Turbine, and battery systems, *Engineering* **6**, 812–826 (2020)
10. H. Mehrjerdi, Modeling, integration, and optimal selection of the Turbine technology in the hybrid wind-photovoltaic renewable energy system design, *Energy Convers. Manag.* **205**, 112350 (2020)
11. P. Mohan Kumar, K. Sivalingam, T.C. Lim, S. Ramakrishna, H. Wei, Strategies for enhancing the low wind speed performance of H-Darrieus wind turbine—Part 1, *Clean Technol.* **1**, 185–204 (2019)
12. K. Venkatraman, S. Moreau, J. Christophe, C. Schram, Numerical investigation of h-Darrieus wind turbine aerodynamics at different tip speed ratios, *Int. J. Numer. Methods Heat Fluid Flow* **33**, 1489–1512 (2023)
13. M. Asadi, R. Hassanzadeh, Assessment of Bach-type internal rotor on the performance of a hybrid wind turbine: effects of attachment angle, tip speed ratio, and free-wind speed, *Int. J. Green Energy* 1–19 (2023)
14. R.W. Zhao, A.C. Creech, Y. Li, V. Venugopal, A.G. Borthwick, Numerical analysis of the performance of a three-bladed vertical-axis turbine with active pitch control using a coupled unsteady Reynolds-averaged Navier-Stokes and actuator line model *J. Hydrodyn.* **35**, 516–532 (2023)

15. K. Vimalakanthan, H. van der Mijle Meijer, I. Bakhmet, G. Schepers, Computational fluid dynamics (CFD) modelling of actual eroded wind turbine blades, *Wind Energ. Sci.* **8**, 41–69 (2023)
16. S. Abdelhady, Techno-economic study and the optimal hybrid renewable energy system design for a hotel building with net zero energy and net zero carbon emissions, *Energy Convers. Manag.* **289**, 117195 (2023)
17. H.T. Hossain, S. Al Faiyaz, A.H. Mridul, M.A. Hossain, K.J. Ahmed, Cost analysis of an optimized hybrid energy system for a remote area in St. John's, NL, *Energy Syst. Res.* **6**, 5–13 (2023)
18. W.R. Nyemba, S. Chinguwa, I. Mushanguri, C. Mbohwa, Optimization of the design and manufacture of a solar-wind hybrid street light, *Procedia Manuf.* **35**, 285–290 (2019)
19. A. Hosseini, N. Goudarzi, Design and CFD study of a hybrid vertical-axis wind Turbine by employing a combined bach-type and H-darrieus rotor systems, *Energy Convers. Manag.* **189**, 49–59 (2019)
20. O.S. Mohamed, A.M.R. Elbaz, A. Bianchini, A better insight on physics involved in the self-starting of a straight-blade darrieus wind Turbine by means of two-dimensional computational fluid dynamics, *J. Wind Eng. Ind. Aerodyn.* **218**, 104793 (2021)
21. Mutombo, N. Marc Alain, B.P. Numbi, Assessment of renewable energy potential in Kwazulu-Natal province, South Africa, *Energy Rep.* **5**, 874–881 (2019)
22. M. Ahmad, A. Shahzad, F. Akram, F. Ahmad, S. I. A. Shah, Design optimization of double-darrieus hybrid vertical axis wind turbine, *Ocean Eng.* **254**, 111171 (2022)
23. S. Ali, C.M. Jang, Effects of tip speed ratios on the blade forces of a small H-darrieus wind turbine, *Energies* **14**, 1–18 (2021)
24. S. Akhlaghi, H. Sangrody, M. Sarailoo, M. Rezaeiahari, Efficient operation of residential solar panels with determination of the optimal tilt angle and optimal intervals based on forecasting model, *IET Renew. Power Gener.* **11**, 1261–67 (2017)
25. S. Li, Y. Li, C. Yang, Q. Wang, B. Zhao, D. Li, R. Zhao, T. Ren, X. Zheng, Z. Gao, W. Xu, Experimental investigation of solidity and other characteristics on dual vertical axis wind Turbines in an urban environment, *Energy Convers. Manag.* **229** (2021). Doi: [10.1016/j.enconman.2020.113689](https://doi.org/10.1016/j.enconman.2020.113689)
26. J. Yang, Z. Yang, Y. Duan, Optimal capacity and operation strategy of a solar-wind hybrid renewable energy system, *Energy Convers. Manag.* **244**, 114519 (2021)
27. F.B. Ismail, N.F.O. Al-Muhsen, N.I. Noruddin, Design and development of dual power generation solar and windmill generator, *Int. J. Electr. Electron. Eng. Telecommun.* **9**, 447–454 (2020)
28. M.F. Francis, O.O. Ajayi, J.O. Ojo, Development of novel airfoil for low wind speed vertical axis wind turbine using Q-blade simulation tool, *Fuel Commun.* **9**, 100028 (2021)
29. A. Hussain, M. Panhwar, S. Hussain, M. Shaikh, U. Zaffar, Efficiency analysis of a small vertical axis wind Turbine using Q-blade, in: *6th International Conference on Energy, Environment and Sustainable Development*, 2022, Vol. 2022, pp. 9–20
30. M.A. Dabachi, A. Rahmouni, O. Bouksour, Design and aerodynamic performance of new floating H-darrieus vertical axis wind Turbines, *Mater. Today: Proc.* **30**, 899–904 (2019)
31. N.P. Noronha, M. Krishna, Aerodynamic performance comparison of airfoils suggested for small horizontal axis wind Turbines, *Mater. Today: Proc.* **46**, 2450–2455 (2021)
32. I. Hashem, M.H. Mohamed, Aerodynamic performance enhancements of H-rotor darrieus wind Turbine. *Energy* **142**, 531–545 (2018)
33. J.F. Manwell, J.G. McGowan, A.L. Rogers, *Wind Energy Explained: Theory, Design and Application* (JOHN WILEY & SONS, INC, 2010)
34. W.A. Eltayeb, J. Somlal, S. Kumar, S.K. Rao, Design and analysis of a solar-wind hybrid renewable energy tree, *Results Eng.* **17**, 100958 (2023)
35. B.N. Sharath, K.S. Madhu, D.G. Pradeep, P. Madhu, B.G. Premkumar, S. Karthik, Conjectured hybrid power with artificial intelligence and single-axis solar tracking wind Turbine, *Int. J. Energ. Water Resour.* 1–7 (2023)
36. P.V. Manusmare, U.G. Bonde, D.A. Bawane, Modeling of hybrid renewable energy system, *Int. J. Res. Appl. Sci. Eng. Technol. (IJRASET)* **11**, 1226–1231 (Bawane)
37. K. Muchiri, J.N. Kamau, D.W. Wekesa, C.O. Saoko, J.N. Mutuku, J.K. Gathua, Wind and solar resource complementarity and its viability in wind/PV hybrid energy systems in Machakos, Kenya, *Sci. Afr.* **20**, e01599 (2023)
38. B. Sakti, R.M. Utomo, A.E. Burhandenny, I.R.S. Siregar, A. Ridho, Simulation of the use of solar and wind energy as a hybrid power plant in malahing village using software homer, in: *International Conference of Tropical Studies and its Applications (ICTROPS 2022)*, 2023, July, Atlantis Press, pp. 351–364
39. B. Charpota, S.K. Sharma, Power quality enhancement in a solar-wind hybrid energy generation system connected to a standalone micro-grid, *Int. J. Eng. Appl. Sci. Technol.* **8**, 89–99 (2023)

Cite this article as: Firas Basim Ismail Alnaimi, Hussein A. Kazem, Ariff Bin Alzakri, Abdulaziz Mohammed Alatir, Design and implementation of smart integrated hybrid Solar-Darrieus wind turbine system for in-house power generation, *Renew. Energy Environ. Sustain.* **9**, 2 (2024)